Journal of Power Sources 194 (2009) 737–745

Contents lists available at ScienceDirect

Journal of Power Sources

journal homepage: www.elsevier.com/locate/jpowsour

Composition dependence of ternary Pt–Ni–Cr catalyst activity for the methanol electro-oxidation reaction

Min Ku Jeon, Paul J. McGinn*

Department of Chemical and Biomolecular Engineering, University of Notre Dame, 178 Fitzpatrick, Notre Dame, IN 46556, United States

ARTICLE INFO

Article history:
Received 28 April 2009
Received in revised form 5 June 2009
Accepted 8 June 2009
Available online 17 June 2009

Keywords:
Methanol electro-oxidation
Direct methanol fuel cell
Electrocatalyst
Cyclic voltammetry
Chronoamperometry
Combinatorial chemistry

ABSTRACT

Various compositions of binary and ternary Pt–Ni–Cr alloys were investigated as catalysts for the methanol electro-oxidation reaction (MOR). Among the binary ($Pt_{28}Ni_{72}$/C and $Pt_{28}Cr_{72}$/C) and ternary Pt–Ni–Cr catalysts ($Pt_{28}Ni_{36}Cr_{36}$/C, $Pt_{22}Ni_{39}Cr_{39}$/C, $Pt_{33}Ni_{31}Cr_{36}$/C, and $Pt_{33}Ni_{36}Cr_{31}$/C) examined, the $Pt_{28}Ni_{36}Cr_{36}$/C composition exhibited the highest MOR mass activity (4.42 A $g_{cat.}^{-1}$) in the as-prepared version, which was higher than the 3.58 A $g_{cat.}^{-1}$ value of the PtRu/C catalyst after 60 min of chronoamperometry testing. The order of mass activity for the MOR was $Pt_{28}Ni_{36}Cr_{36}$/C > $Pt_{33}Ni_{36}Cr_{31}$/C > $Pt_{22}Ni_{39}Cr_{39}$/C > $Pt_{33}Ni_{31}Cr_{36}$/C > $Pt_{28}Cr_{72}$/C > $Pt_{28}Ni_{72}$/C, which was slightly changed to $Pt_{28}Ni_{36}Cr_{36}$/C > $Pt_{22}Ni_{39}Cr_{39}$/C > $Pt_{33}Ni_{36}Cr_{31}$/C > $Pt_{33}Ni_{31}Cr_{36}$/C > $Pt_{28}Cr_{72}$/C > $Pt_{28}Ni_{72}$/C after a conditioning process. The effect of anodic conditioning was also studied. A combination of X-ray diffraction, cyclic voltammetry, and chronoamperometry experiments revealed that the conditioning process caused dissolution and an oxidation state change of metallic Ni and Cr_2O_3 in the binary catalysts. The higher MOR mass activities of the ternary catalysts compared to the binary ones is attributed to co-alloying of Ni and Cr, leading to exposure of more Pt on the catalyst surface without reducing specific activities of the catalysts. The results of this study also correlate well with a prior ranking of catalytic activity of the same compositions in the form of thin film catalysts that we processed and evaluated by a high-throughput combinatorial approach [J.S. Cooper, M.K. Jeon, P.J. McGinn, Electrochem. Commun. 10 (2008) 1545–1547].

1. Introduction

Methanol electro-oxidation reaction (MOR) catalysts are under intensive study for direct methanol fuel cells (DMFCs) application. Unlike other types of fuel cells which use hydrogen as an anode reactant, DMFCs use methanol as the anode fuel. The use of liquid fuel allows for easy fuel handling and reduced re-fueling time. These merits make DMFCs a promising alternative for lithium-ion batteries for portable applications [1]. Although the performance of DMFCs has been strongly improved during the last two decades, DMFCs still suffer from low catalytic activity of the anode and cathode catalysts, and methanol cross-over from the anode to the cathode electrode.

Initially, Pt was employed as the MOR catalyst in DMFCs, but a rapid decrease of activity was observed because of poisoning by intermediate CO [1]. CO tolerance was significantly improved by introducing a Pt–Ru alloy catalyst [2–5]. Pt–Ru is still widely used, but a desire for greater MOR activity and reduced costs have led to a continued search for alternative catalysts. Most researchers have focused on Pt–Ru based catalysts [6–8] including PtRuFe [9,10], PtRuNi [11,12], PtRuCo [13–15], PtRuW [14–17], and PtRuMo [16,18] to achieve both improved MOR activity and reduced costs. However, recent reports on the performance degradation of DMFCs show that dissolution of Ru occurs during long-term operation [19,20] and that the dissolved Ru crosses through the membrane and are reduced on the cathode electrode resulting in performance decrease [21,22]. Thus more research on Ru-free MOR catalysts is desirable. There are only a limited number of reports on Ru-free MOR catalysts, with promising results being reported in Pt–Co, Pt–Ni, Pt–Fe [23], Pt–Pb [24–26], Pt–Ni–Cr [27–29], and Pt–Co–Cr [30] alloy systems.

Previously, we investigated ternary Pt–Ni–Cr alloys as candidate catalysts for the MOR via a thin film combinatorial method and followed this with an examination of powder versions of the best catalyst compositions [27–29]. It was shown that $Pt_{28}Ni_{36}Cr_{36}$ composition exhibits satisfactory performance for the MOR that was comparable to that of a PtRu/C catalyst. A thin film combinatorial method is a powerful tool to explore many compositions quickly, but it needs to be complemented by other studies because the synthesis and characterization methods used in the combinatorial libraries are different from conventional techniques used for powder versions of catalysts as typically employed in fuel cells [31,32].

* Corresponding author. Tel.: +1 574 631 6151; fax: +1 574 631 8366.
E-mail address: mcginn.1@nd.edu (P.J. McGinn).

0378-7753/$ – see front matter © 2009 Elsevier B.V. All rights reserved.
doi:10.1016/j.jpowsour.2009.06.019

In our earlier Pt–Ni–Cr catalyst study [27], we used multi-target sputtering to synthesize multi-layers of Pt, Ni, and Cr. The multi-layers were annealed to form homogeneous alloys and then characterized simultaneously in a multichannel multielectrode analyzer. The follow-up powder version of the best thin film catalyst composition was synthesized by a chemical reduction method and then characterized by conventional methods such as cyclic voltammetry (CV) and chronoamperometry (CA) experiments. In that study only the best thin film composition was examined. Hence it is natural to consider a range of powder compositions around the best thin film composition to investigate if the different synthesis/characterization techniques yield different optima and provide further validation of the thin film approach. Differences between powder and thin film performance might arise due to differing surface properties such as composition or the oxidation states of Ni and Cr.

Thus the present study examines if the best composition identified via a thin film combinatorial approach is also the best among a range of powder compositions. Various compositions of ternary ($Pt_{28}Ni_{36}Cr_{36}$, $Pt_{22}Ni_{39}Cr_{39}$, $Pt_{33}Ni_{31}Cr_{36}$, and $Pt_{33}Ni_{36}Cr_{31}$ compositions) and binary ($Pt_{28}Ni_{72}$ and $Pt_{28}Cr_{72}$) catalysts from the Pt–Ni–Cr systems were synthesized and characterized. In addition, the effect of an anodic conditioning process was also investigated. The conditioning process was previously introduced in thin film library studies to improve the MOR activity [14]. The activity improvement was subsequently also observed in powder versions of a Pt–Ni–Cr catalyst [29] indicating that the conditioning process is beneficial to achieve higher MOR activity.

2. Experimental methods

2.1. Catalysts synthesis

All the Pt–Ni–Cr catalysts were synthesized by a conventional $NaBH_4$ reduction method [33]. $H_2PtCl_6{\cdot}6H_2O$, $NiCl_2$, and $Cr(NO_3)_3{\cdot}9H_2O$ were used as Pt, Ni, and Cr precursors, respectively. The precursors were dissolved in a mixture of de-ionized (DI) water and isopropyl alcohol (80:1 volume ratio). Carbon support (Vulcan XC 72R) was added to the mixture. The mixture was sonicated and stirred for 30 min to achieve homogeneous mixing. 0.2 M $NaBH_4$ solution was added to the mixture as a reducing agent. Previously, we have shown that the amount of reducing agent, $NaBH_4$, affects catalytic properties of the PtNiCr catalysts [28], and the highest MOR activity was observed when 50 times the stoichiometric amount of $NaBH_4$ was applied. In this study, the amount

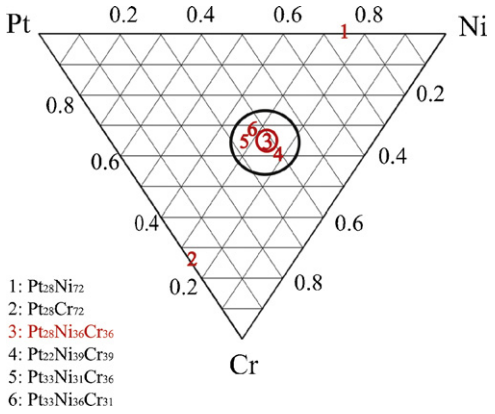

Fig. 1. Map of the synthesized catalyst compositions: $Pt_{28}Ni_{72}$/C, $Pt_{28}Cr_{72}$/C, $Pt_{28}Ni_{36}Cr_{36}$/C, $Pt_{22}Ni_{39}Cr_{39}$/C, $Pt_{33}Ni_{31}Cr_{36}$/C, and $Pt_{33}Ni_{36}Cr_{31}$/C. The encircled composition range investigated in this study was identified as the region of highest activity in thin film screening [27]. Point '3' is the composition $Pt_{28}Ni_{36}Cr_{36}$, which showed the highest MOR activity in the thin film library.

of 0.2 M $NaBH_4$ solution was fixed as 50 times the stoichiometric amount for all samples except for the Pt/C and PtRu/C catalysts. The mixture was further stirred for 1 h to complete the reduction reaction. All reactions were performed at room temperature. The final mixture was filtered and washed with DI water. The resulting powder was dried at 100 °C in an oven overnight. Total metal loading was adjusted to 20 wt.% of the total catalyst mass. The synthesized catalysts were named according to their composition so, for example, $Pt_{28}Ni_{36}Cr_{36}$/C represents a molar ratio of Pt:Ni:Cr of 28:36:36. Synthesized ternary and binary catalyst compositions are: $Pt_{28}Ni_{36}Cr_{36}$/C, $Pt_{22}Ni_{39}Cr_{39}$/C, $Pt_{33}Ni_{31}Cr_{36}$/C, $Pt_{33}Ni_{36}Cr_{31}$/C, $Pt_{28}Ni_{72}$/C, and $Pt_{28}Cr_{72}$/C. A composition map is shown in Fig. 1. Pt/C and $Pt_{50}Ru_{50}$/C ("PtRu/C") catalysts were also synthesized by the same method for comparison except that the amount of 0.2 M $NaBH_4$ solution differed (5 times of stoichiometric amount was applied as it was determined to be the best ratio for PtRu/C [33]). Previously obtained results for these compositions are used in this study [28].

2.2. Structural and electrochemical characterization of the catalysts

Structural characteristics of the catalysts were measured by X-ray diffraction (XRD) over a 2θ range of 20–80° in a step scan mode (0.02° step size and 0.5 s duration time for each step).

For electrochemical analysis, working electrodes were prepared by the thin film method [34]. The catalysts were dispersed in a mixture of DI water and 5 wt.% Nafion ionomer solution. The dispersion was sonicated to achieve homogeneous mixing and then a small amount of the dispersion was dripped on a glassy carbon electrode (3 mm dia., BAS Co., Ltd., MF-2012). After drying in the air, 5 wt.% Nafion ionomer solution was dripped on the catalyst layer to stabilize it. Electrochemical testing was performed in a beaker-type three electrode cell. Pt mesh and saturated calomel electrode were employed as the counter and reference electrodes, respectively. MOR activities were measured via chronoamperometry (CA) tests by keeping the working electrodes at 0.6 V (vs. reversible hydrogen electrode, RHE) for 1 h. All potentials in this paper were converted into RHE scale.

2.3. Conditioning process

Before the conditioning process, the catalysts were rapidly annealed in a tube furnace at 900 °C for 5 min under H_2/Ar (5.2 mol.% H_2) flow to get a higher degree of alloying, with rapid insertion under atmosphere achieved using an external magnetic coupling device. This condition is very close to the previously reported annealing process employed for the Pt–Ni–Cr combinatorial library (900 °C for 5 min under vacuum) [27]. The conditioning process was performed by potential cycling between −0.06 and 1.34 V (vs. RHE) for 10 cycles at a scan rate of 10 mV s^{-1} and 60 °C. Cyclic voltammetry (CV) was measured by potential cycling between 0 and 1.2 V (vs. RHE) for 3 cycles before and after the conditioning processes. The MOR activities were also measured before and after the conditioning processes by the CA tests mentioned above. The 900 °C annealed catalysts were denoted by adding "−900" after their initial name (for example, "$Pt_{28}Ni_{36}Cr_{36}$/C-900").

3. Results and discussion

3.1. Pt–Ni and Pt–Cr binary catalysts

Fig. 2 shows the XRD results of binary $Pt_{28}Ni_{72}$/C and $Pt_{28}Cr_{72}$/C catalysts before and after the 900 °C annealing process. Results for pure Pt are also included for comparison [28]. In the $Pt_{28}Ni_{72}$/C and

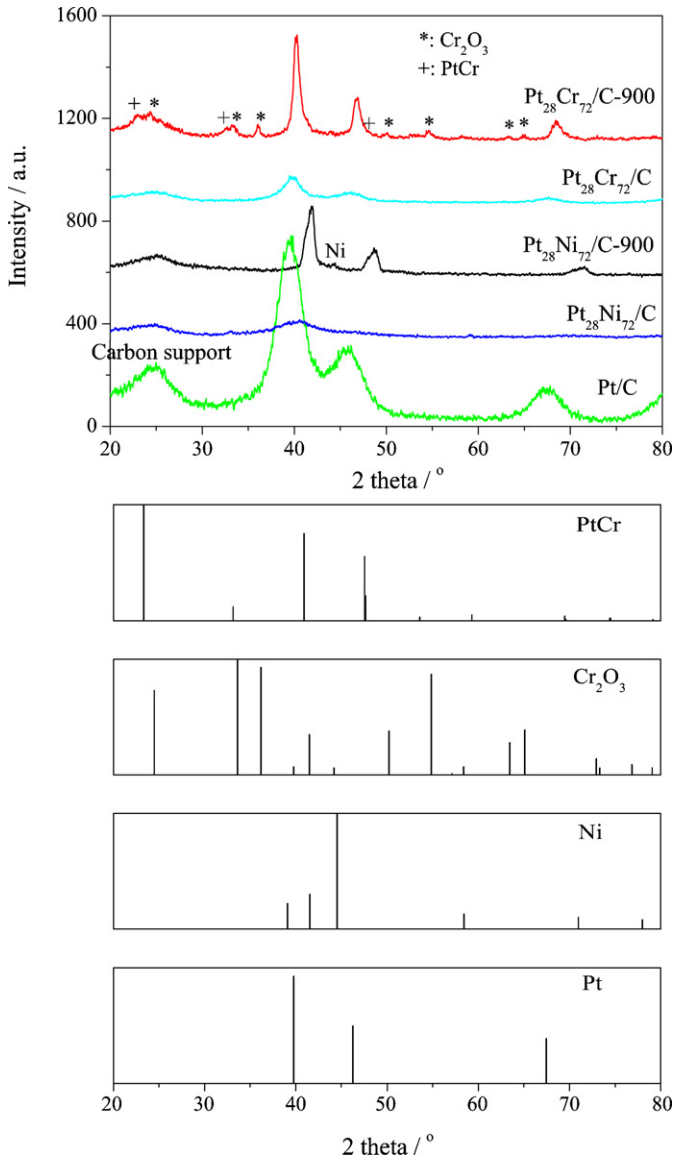

Fig. 2. The XRD patterns of the $Pt_{28}Ni_{72}$/C, $Pt_{28}Ni_{72}$/C-900, $Pt_{28}Cr_{72}$/C, and $Pt_{28}Cr_{72}$/C-900 catalysts. Prior data of Pt/C is also included [28]. PtCr peaks are denoted by '+' and Cr_2O_3 peaks are denoted by '*'. Peak positions and intensities of Pt (ICDD 65-2868), Ni (ICDD 45-1027), Cr_2O_3 (ICDD 38-1479), and PtCr (ICDD 34-0707) are also shown.

$Pt_{28}Cr_{72}$/C catalysts, only fcc Pt peaks were observed. The peak position of the (1 1 1) peak moved from 39.48° in the pure Pt/C [28] to 40.40 and 39.81° for the $Pt_{28}Ni_{72}$/C and $Pt_{28}Cr_{72}$/C catalysts, respectively, indicating slight alloying of Ni and Cr with Pt. The (1 1 1) peak position further shifted in the $Pt_{28}Ni_{72}$/C-900 and $Pt_{28}Cr_{72}$/C-900 catalysts to 41.76 and 40.14°, respectively, which means a higher degree of alloying was achieved via 900 °C annealing. While we could not observe any impurity peaks in the non-annealed $Pt_{28}Ni_{72}$/C and $Pt_{28}Cr_{72}$/C catalysts, new peaks appeared in the annealed catalysts. In the $Pt_{28}Ni_{72}$/C-900 catalyst, a peak corresponding to metallic Ni was observed, which is denoted in Fig. 2. Peaks corresponding to PtCr (denoted by '+' in Fig. 2) and Cr_2O_3 (denoted by '*' in Fig. 2) were observed in the $Pt_{28}Cr_{72}$/C-900 catalyst. These results mean that the annealing condition (at 900 °C for 5 min under 5.2 mol.% H_2/Ar flow) was not sufficient to reduce Cr_2O_3 while Ni was reduced to metallic form. Crystallite sizes of the catalysts were calculated by the Scherrer equation [35], and the results were 1.7 and 3.7 nm for the $Pt_{28}Ni_{72}$/C and $Pt_{28}Cr_{72}$/C catalysts, respectively. The crystallite sizes increased to 8.7 and 8.8 nm in the $Pt_{28}Ni_{72}$/C-900 and $Pt_{28}Cr_{72}$/C-900 catalysts, respectively. A summary of the XRD results is listed in Table 1.

Table 1
Summary of the XRD results of the PtNi, PtCr, and ternary Pt–Ni–Cr catalysts. Results of pure Pt were also included [28].

Catalyst	(1 1 1) peak position/°	d/nm	Lattice parameter/nm	Crystallite size/nm
Pt (Ref. [28])	39.48	0.2281	0.3951	2.6
$Pt_{28}Ni_{72}$/C	40.40	0.2231	0.3864	1.7
$Pt_{28}Ni_{72}$/C-900	41.76	0.2161	0.3743	8.7
$Pt_{28}Cr_{72}$/C	39.81	0.2263	0.3920	3.7
$Pt_{28}Cr_{72}$/C-900	40.14	0.2245	0.3888	8.8
$Pt_{28}Ni_{36}Cr_{36}$/C (Ref. [28])	39.51	0.2279	0.3947	1.1
$Pt_{28}Ni_{36}Cr_{36}$/C-900	42.13	0.2143	0.3712	12.2
$Pt_{22}Ni_{39}Cr_{39}$/C	39.53	0.2278	0.3946	0.8
$Pt_{22}Ni_{39}Cr_{39}$/C-900	42.13	0.2143	0.3718	20.1
$Pt_{33}Ni_{31}Cr_{36}$/C	40.60	0.2220	0.3845	0.7
$Pt_{33}Ni_{31}Cr_{36}$/C-900	41.58	0.2170	0.3759	8.5
$Pt_{33}Ni_{36}Cr_{31}$/C	39.56	0.2276	0.3942	1.0
$Pt_{33}Ni_{36}Cr_{31}$/C-900	41.85	0.2157	0.3736	19.3

The CV results of the $Pt_{28}Ni_{72}$/C and $Pt_{28}Cr_{72}$/C catalysts are shown in Fig. 3 with previously reported CV results of Pt/C [28] and PtRu/C [36] catalysts. The PtRu/C catalyst exhibited poorly defined H^+ desorption peaks (0–0.3 V along positive scan direction) due to Ru alloying. But the $Pt_{28}Ni_{72}$/C and $Pt_{28}Cr_{72}$/C catalysts showed a Pt-like shape in the CV tests in the H^+ adsorption/desorption region (0–0.3 V). This result indicates a low degree of alloying was achieved via the $NaBH_4$ reduction method, which is in line with the XRD results. Electrochemically active surface area (EAS) values were calculated from the desorption area of H^+ by using 210 μC cm^{-1} for monolayer charge. It should be noted that this value is based on polycrystalline Pt [37] and is not precise in alloy catalysts. Although the absolute values may not be correct, the EAS values are still useful for evaluation of relative specific activities which is an important property of electrocatalysts. The EAS values were 7.96, 1.78, 2.51 and 2.01 m^2 $g_{cat.}^{-1}$ for the Pt/C, PtRu/C, $Pt_{28}Ni_{72}$/C and $Pt_{28}Cr_{72}$/C catalysts, respectively, including previous results for the Pt/C and PtRu/C catalysts [28]. In spite of low Pt content, the $Pt_{28}Ni_{72}$/C and $Pt_{28}Cr_{72}$/C catalysts showed larger EAS values than that of the PtRu/C catalyst suggesting that the catalyst surface is enriched in Ru during the $NaBH_4$ reduction.

Fig. 4(a) shows the CA results of the $Pt_{28}Ni_{72}$/C and $Pt_{28}Cr_{72}$/C catalysts. The results of the PtRu and $Pt_{28}Ni_{36}Cr_{36}$ catalysts which were reported previously are also shown for comparison [28,29].

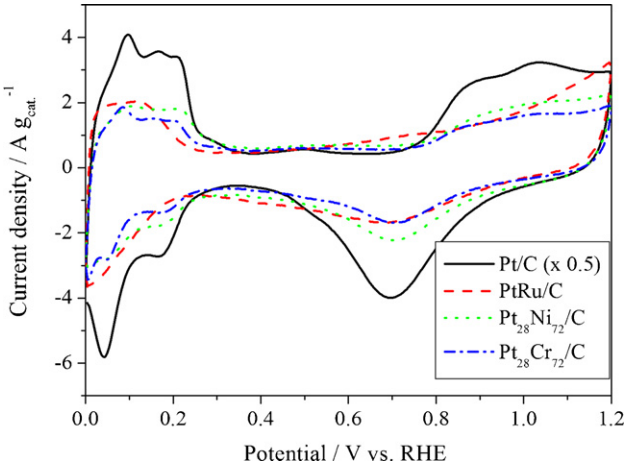

Fig. 3. Cyclic voltammetry test results of the Pt/C, PtRu/C, $Pt_{28}Ni_{72}$/C, and $Pt_{28}Cr_{72}$/C catalysts. 0.5 M H_2SO_4 solution was used as the electrolyte. The scan rate was 50 mV s^{-1}. The scale of the results from the Pt/C catalyst was halved for convenience.

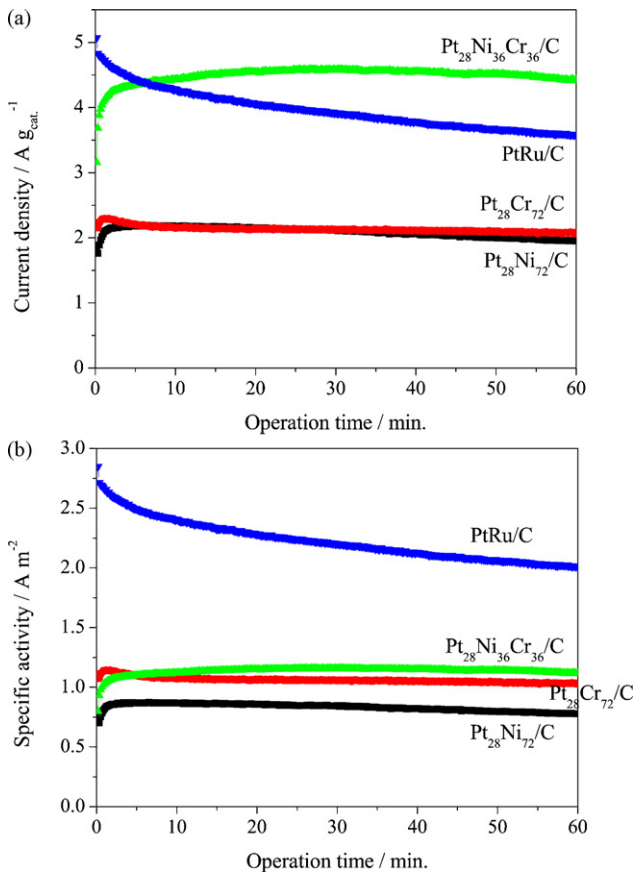

Fig. 4. Chronoamperometry test results of the PtRu/C, $Pt_{28}Ni_{72}$/C, $Pt_{28}Cr_{72}$/C, and $Pt_{28}Ni_{36}Cr_{36}$/C catalysts performed by keeping the working electrode at 0.6 V (vs. RHE) for 60 min 1 M H_2SO_4 + 1 M methanol solution was used as the electrolyte. Both (a) g-catalyst and (b) EAS based activities are shown.

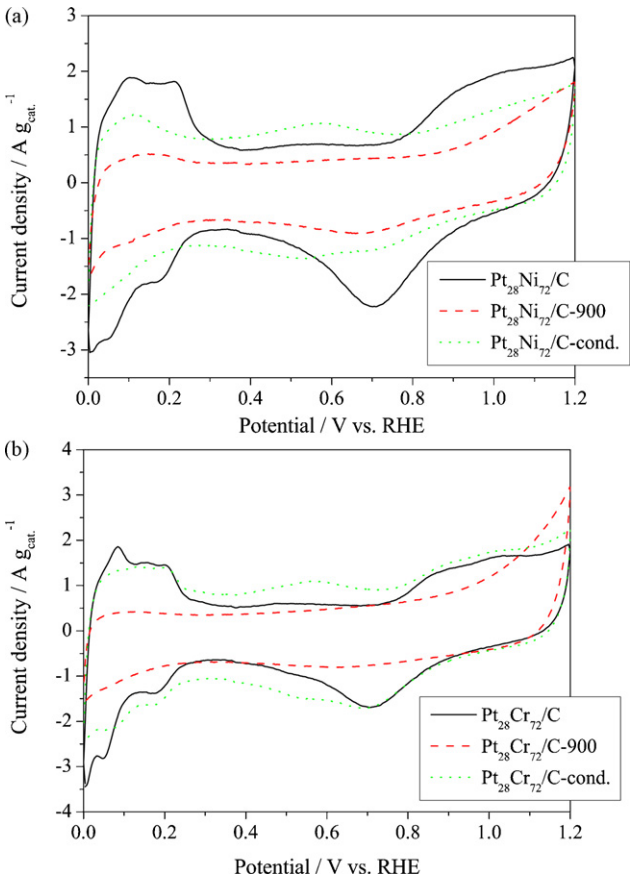

Fig. 5. Cyclic voltammetry results of the (a) $Pt_{28}Ni_{72}$ catalysts and (b) $Pt_{28}Cr_{72}$ catalysts before and after 900 °C annealing and the conditioning process. 0.5 M H_2SO_4 solution was used as the electrolyte. Scan rate was 50 mV s^{-1}.

Both of the binary catalysts exhibited much lower current density after 60 min operation (1.95 and 2.08 A $g_{cat.}^{-1}$ for the $Pt_{28}Ni_{72}$/C and $Pt_{28}Cr_{72}$/C, respectively) than the 4.42 and 3.58 A $g_{cat.}^{-1}$ values in the $Pt_{28}Ni_{36}Cr_{36}$/C and PtRu/C catalysts, respectively. Specific activities derived by dividing the CA results by electrochemically active surface area (EAS) are shown in Fig. 4(b). Like the mass activity results, specific activity of the $Pt_{28}Ni_{36}Cr_{36}$/C catalyst (1.12 A m^{-2} at 60 min of operation) was superior to 0.779 and 1.03 A m^{-2} in the $Pt_{28}Ni_{72}$/C and $Pt_{28}Cr_{72}$/C catalysts, respectively. These results prove a synergistic effect from the co-addition of Ni and Cr into the Pt catalyst, while Cr is more beneficial than Ni to achieve higher MOR in Pt based binary alloys.

The effect of conditioning was investigated via CV tests before and after the conditioning process. The CV results of the $Pt_{28}Ni_{72}$/C, $Pt_{28}Ni_{72}$/C-900, and $Pt_{28}Ni_{72}$/C-cond. catalysts are shown in Fig. 5(a). The H^+ adsorption/desorption peaks are largely reduced after the 900 °C anneal, while they were significantly recovered after the conditioning process because of surface Ni dissolution. EAS values of the $Pt_{28}Ni_{72}$/C-900 and $Pt_{28}Ni_{72}$/C-cond. catalysts were 0.203 and 0.501 m^2 $g_{cat.}^{-1}$, respectively, which were only 8.1 and 20.0% of 2.51 m^2 $g_{cat.}^{-1}$ in the $Pt_{28}Ni_{72}$/C catalyst. The EAS value was not fully recovered after the conditioning process due to the increase of crystallite size. The CV results of the $Pt_{28}Cr_{72}$/C, $Pt_{28}Cr_{72}$/C-900, and $Pt_{28}Cr_{72}$/C-cond. catalysts are shown in Fig. 5(b), which also exhibited suppressed H^+ adsorption/desorption after the 900 °C anneal. But exposure of the Pt surface was more significant than the case of the PtNi catalysts. EAS values of the $Pt_{28}Cr_{72}$/C-900 and $Pt_{28}Cr_{72}$/C-cond. catalysts were 0.0720 and 0.962 m^2 $g_{cat.}^{-1}$, respectively. When compared with the results of the PtNi catalysts, the increase of EAS via the conditioning process is much larger in the $Pt_{28}Cr_{72}$/C-cond. catalyst (1240%) than that in the $Pt_{28}Ni_{72}$/C-cond. catalyst (147%), which means significant dissolution of Cr_2O_3 occurs. In addition, it should be noted that the EAS value of the $Pt_{28}Cr_{72}$/C-900 (0.0720 m^2 $g_{cat.}^{-1}$) was much smaller than the 0.203 m^2 $g_{cat.}^{-1}$ value in the $Pt_{28}Ni_{72}$/C-900 catalyst, while that of $Pt_{28}Cr_{72}$/C-cond. is 92% higher than that of the $Pt_{28}Ni_{72}$/C-cond. catalyst. This result shows more significant surface segregation and dissolution of Cr_2O_3 during the annealing and conditioning process, respectively.

The effect of the conditioning on the MOR activity was measured by employing CA tests, and the results are shown in Fig. 6(a). At 60 min operation, the MOR activities of the $Pt_{28}Ni_{72}$/C-900 and $Pt_{28}Cr_{72}$/C-900 catalysts were 0.214 and 0.134 A $g_{cat.}^{-1}$, respectively, which increased dramatically to 0.733 and 2.12 A $g_{cat.}^{-1}$ in the $Pt_{28}Ni_{72}$/C-cond. and $Pt_{28}Cr_{72}$/C-cond. catalysts, respectively. Specific MOR activities were also compared in Fig. 6(b) based on the EAS values. The specific activities increased from 0.779 and 1.03 A m^{-2} in the $Pt_{28}Ni_{72}$/C and $Pt_{28}Cr_{72}$/C, respectively, to 1.05 and 1.86 A m^{-2} in the $Pt_{28}Ni_{72}$/C-900 and $Pt_{28}Cr_{72}$/C-900, respectively, indicating that a higher degree of alloying is beneficial for the MOR (especially in the Pt–Cr case). After the conditioning tests, the specific activities further increased to 1.46 and 2.20 A m^{-2} in the $Pt_{28}Ni_{72}$/C-cond. and $Pt_{28}Cr_{72}$/C-cond. catalysts, respectively. Although a significant increase of specific activity (39%) was observed in the $Pt_{28}Ni_{72}$/C-cond. catalyst, only an 18% increase in specific activity was shown in the $Pt_{28}Cr_{72}$/C-cond. catalyst. This improvement in the MOR might have been achieved by an oxidation state change of Ni and Cr (Cr_2O_3). And the more significant change in the $Pt_{28}Ni_{72}$/C-cond. catalyst suggests the oxidation state change was more significant in

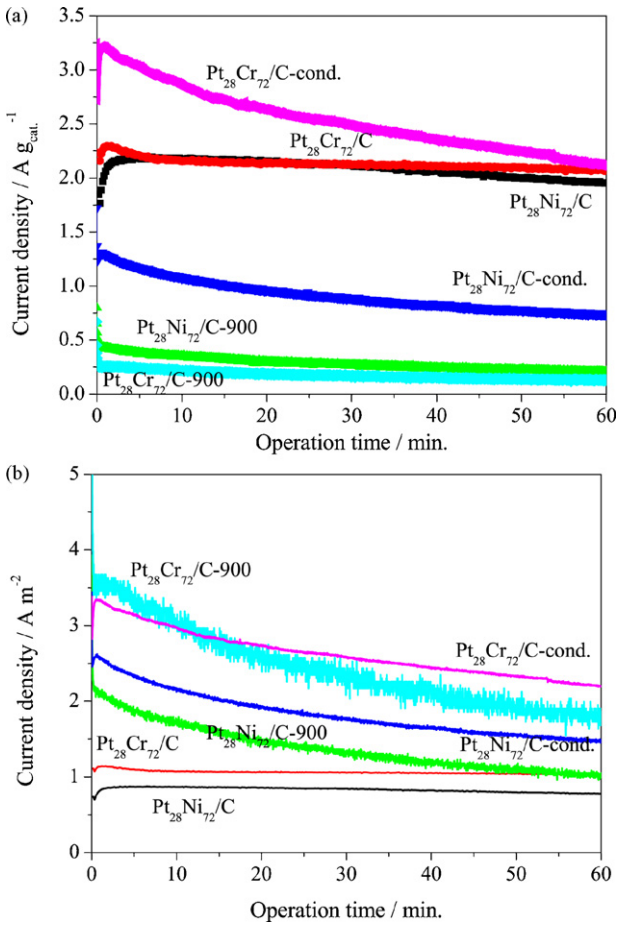

Fig. 6. Chronoamperometry results of the $Pt_{28}Ni_{72}$ and $Pt_{28}Cr_{72}$ catalysts based on (a) catalyst mass ($A\,g_{cat.}^{-1}$) and (b) specific activities ($A\,m^{-2}$). The data were obtained by keeping the working electrodes at 0.6 V (vs. RHE) for 60 min in the 1 M methanol + 1 M H_2SO_4 electrolyte.

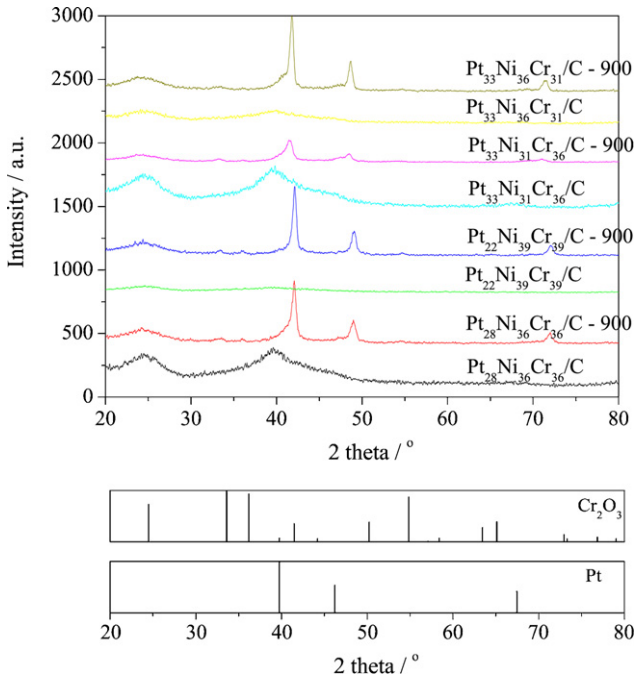

Fig. 7. The XRD patterns of ternary PtNiCr catalysts including 900 °C annealed catalysts. Reference peaks for pure Pt (ICDD 65-2868) and Cr_2O_3 (ICDD 38-1479) phases are also shown.

metallic Ni than in Cr_2O_3. In the above, it is seen that the EAS values increased by 147 and 1240% in the $Pt_{28}Ni_{72}$/C-cond. and $Pt_{28}Cr_{72}$/C-cond. catalysts, respectively. Therefore, it can be concluded that the increase in the MOR mass activity of both the $Pt_{28}Ni_{72}$/C-cond. and $Pt_{28}Cr_{72}$/C-cond. catalysts came from dissolution and oxidation state change of metallic Ni and Cr_2O_3, but the contribution of dissolution and oxidation state change on each catalyst is different. In addition, it should be noted that, in spite of significant dissolution of Cr_2O_3 in the $Pt_{28}Cr_{72}$/C-cond. catalyst, the specific activity of the $Pt_{28}Cr_{72}$/C-cond. catalyst is still 51% higher than that of the $Pt_{28}Ni_{72}$/C-cond. catalyst, which means Cr is a better choice than Ni for high MOR in a Pt-based binary system. A summary of the EAS values and the MOR activities is listed in Table 2.

3.2. Pt–Ni–Cr ternary catalysts

The XRD results of the ternary Pt–Ni–Cr catalysts are shown in Fig. 7 before and after 900 °C annealing. Before the anneal-

Table 2
Summary of the electrochemical testing results obtained by cyclic voltammetry and chronoamperometry (at 0.6 V and 60 min operation) experiments.

Catalyst	EAS/$m^2\,g_{cat.}^{-1}$	Mass activity/$A\,g_{cat.}^{-1}$	Specific activity/$A\,m^{-2}$	Mass activity on g-noble metal scale/$A\,g_{noble\ metal}^{-1}$
PtRu/C (Ref. [28])	1.78	3.58	2.01	17.9
PtRu/C-900	1.60	3.56	2.23	17.8
PtRu/C-cond.	1.40	5.07	3.62	25.4
$Pt_{28}Ni_{72}$/C	2.51	1.95	0.779	17.3
$Pt_{28}Ni_{72}$/C-900	0.203	0.214	1.05	1.90
$Pt_{28}Ni_{72}$/C-cond.	0.501	0.733	1.46	6.50
$Pt_{28}Cr_{72}$/C	2.01	2.08	1.03	17.5
$Pt_{28}Cr_{72}$/C-900	0.0720	0.134	1.86	1.13
$Pt_{28}Cr_{72}$/C-cond.	0.962	2.12	2.20	17.9
$Pt_{28}Ni_{36}Cr_{36}$/C (Ref. [28])	3.96	4.42	1.12	38.2
$Pt_{28}Ni_{36}Cr_{36}$/C-900	0.591	1.09	1.84	9.43
$Pt_{28}Ni_{36}Cr_{36}$/C-cond.	2.11	4.03	1.91	34.9
$Pt_{22}Ni_{39}Cr_{39}$	2.81	3.66	1.30	36.7
$Pt_{22}Ni_{39}Cr_{39}$-900	0.209	0.162	0.775	1.63
$Pt_{22}Ni_{39}Cr_{39}$-cond.	1.66	3.24	1.95	32.5
$Pt_{33}Ni_{31}Cr_{36}$	2.88	3.30	1.15	25.9
$Pt_{33}Ni_{31}Cr_{36}$-900	0.529	0.938	1.77	7.37
$Pt_{33}Ni_{31}Cr_{36}$-cond.	1.49	2.57	1.72	20.2
$Pt_{33}Ni_{36}Cr_{31}$	3.70	3.70	1.00	29.2
$Pt_{33}Ni_{36}Cr_{31}$-900	0.308	0.564	1.83	4.45
$Pt_{33}Ni_{36}Cr_{31}$-cond.	1.32	2.88	2.18	22.7

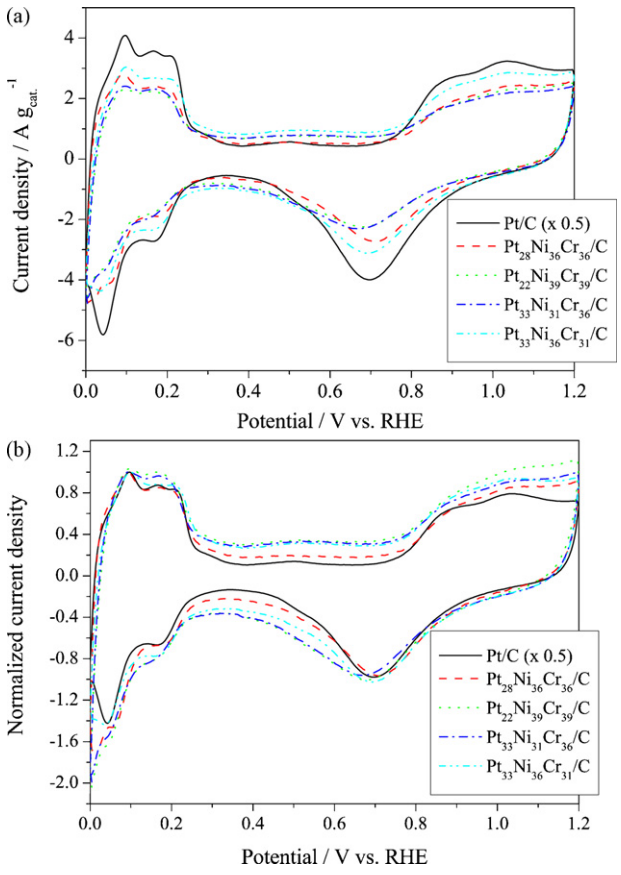

Fig. 8. Cyclic voltammetry results of the $Pt_{28}Ni_{36}Cr_{36}$/C, $Pt_{22}Ni_{39}Cr_{39}$/C, $Pt_{33}Ni_{31}Cr_{36}$/C, and $Pt_{33}Ni_{36}Cr_{31}$/C catalysts based on (a) catalyst mass (A $g_{cat.}^{-1}$) and (b) normalized intensity. That of the Pt/C catalyst was also included with a halved intensity for comparison [28].

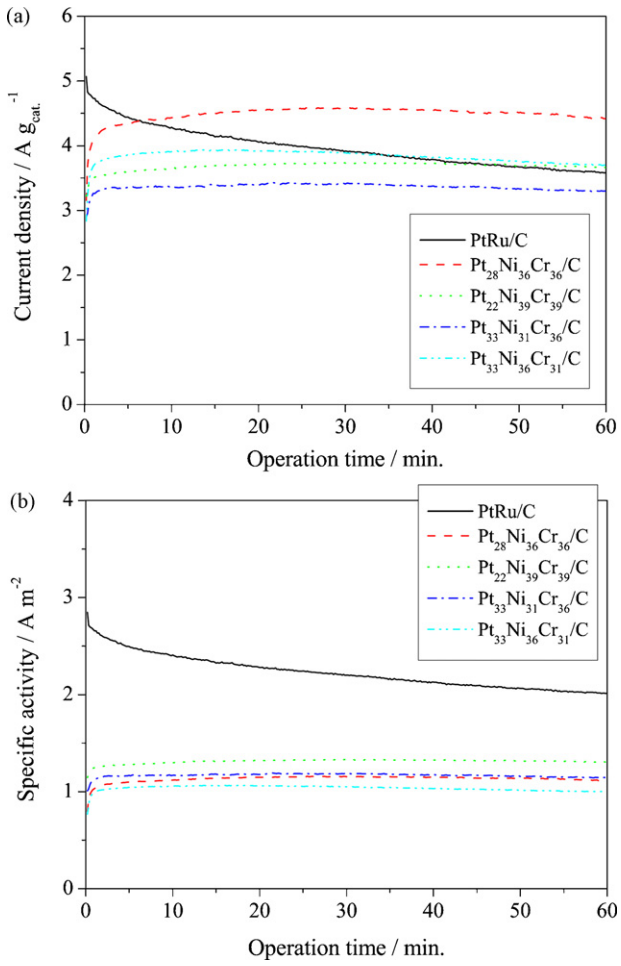

Fig. 9. Chronoamperometry test results of $Pt_{28}Ni_{36}Cr_{36}$/C, $Pt_{22}Ni_{39}Cr_{39}$/C, $Pt_{33}Ni_{31}Cr_{36}$/C, and $Pt_{33}Ni_{36}Cr_{31}$/C catalysts based on (a) catalyst mass (A $g_{cat.}^{-1}$) and (b) specific activity. The tests were performed in 1 M methanol + 1 M H_2SO_4 solution by keeping the working electrode at 0.6 V (vs. RHE) for 60 min.

ing, only fcc Pt peaks were observed without a significant shift of the (1 1 1) peak, indicating formation of a poorly alloyed Pt–Ni–Cr catalyst. After annealing at 900 °C, large shift of the (1 1 1) peak was observed in all samples. In addition, peaks of Cr_2O_3 also appeared in all catalysts although the amount of Cr was nearly half of the $Pt_{28}Cr_{72}$/C catalyst. Crystallite sizes were calculated from the (1 1 1) peaks and the results are listed in Table 1. Before annealing, very small crystallite sizes between 0.1 and 1.1 nm were observed, which means formation of an amorphous phase of poorly alloyed Pt–Ni–Cr is likely. The crystallite size increased after 900 °C annealing to 12.2, 20.1, 8.5, and 19.3 nm for the $Pt_{28}Ni_{36}Cr_{36}$/C-900, $Pt_{22}Ni_{39}Cr_{39}$/C-900, $Pt_{33}Ni_{31}Cr_{36}$/C-900, and $Pt_{33}Ni_{36}Cr_{31}$/C-900 catalysts, respectively. When compared with the 8.7 and 8.8 nm respective sizes of the $Pt_{28}Ni_{72}$/C-900 and $Pt_{28}Cr_{72}$/C-900 catalysts, the ternary catalysts exhibited more coarsening than the binary catalysts. A summary of the XRD results is listed in Table 1.

The CV results of the ternary catalysts are shown in Fig. 8(a). A normalized current density scale (based on peak current density during H^+ desorption) is shown in Fig. 8(b) for convenient comparison. The Pt–Ni–Cr catalysts show a larger capacitive current density (0.3–0.7 V) than that of the Pt/C catalyst, which might be caused by the Ni and Cr_2O_3 phases. EAS values of the catalysts were 3.96, 2.81, 2.88, and 3.70 m^2 $g_{cat.}^{-1}$ for the $Pt_{28}Ni_{36}Cr_{36}$/C, $Pt_{22}Ni_{39}Cr_{39}$/C, $Pt_{33}Ni_{31}Cr_{36}$/C, and $Pt_{33}Ni_{36}Cr_{31}$/C catalysts, respectively.

Fig. 9(a) shows the CA results of ternary catalysts on an A/g-catalyst basis (A $g_{cat.}^{-1}$). The $Pt_{28}Ni_{36}Cr_{36}$/C (4.42 A $g_{cat.}^{-1}$) catalyst showed the highest performance among the ternary catalysts, which was better than the PtRu/C catalyst (3.58 A $g_{cat.}^{-1}$) at 60 min of operation. Other ternary catalysts also exhibited competitive performances, indicating the ternary Pt–Ni–Cr system is a promising candidate for high MOR. On a specific activity scale (A m^{-2}) (shown in Fig. 9(b)), the ternary Pt–Ni–Cr catalysts showed lower activities than that of the PtRu/C catalyst. Interestingly, all of the Pt–Ni–Cr catalysts exhibited similar specific activity in a range of 1.00–1.30 A m^{-2}, indicating that the high activity of the $Pt_{28}Ni_{36}Cr_{36}$/C catalyst came from the large EAS. These results suggest that the $Pt_{28}Ni_{36}Cr_{36}$/C composition is an optimum ratio in terms of exposing Pt on the catalyst surface without losing specific activity, resulting in the highest MOR activity. However, as was mentioned above, the non-annealed catalysts are potentially quite different from our previously reported [27] thin film combinatorial library especially with respect to the degree of alloying and surface oxidation states. Therefore, further experiments were performed as discussed below.

The effect of conditioning was investigated by CV testing, with the results shown in Fig. 10. In all catalysts, H^+ adsorption/desorption peaks increased significantly, indicating exposure of Pt on catalyst surfaces via dissolution of surface Ni and Cr_2O_3. In addition, capacitive currents of the catalysts increased after the conditioning, which might have come from the oxidation state change in the Ni, Cr_2O_3, and carbon support. EAS values were also calculated before and after the conditioning tests as shown in Table 2. The EAS values increased by 182–694% after the conditioning tests, which means extensive dissolution of Ni and Cr_2O_3 species occurred. These increases are within the range of changes observed

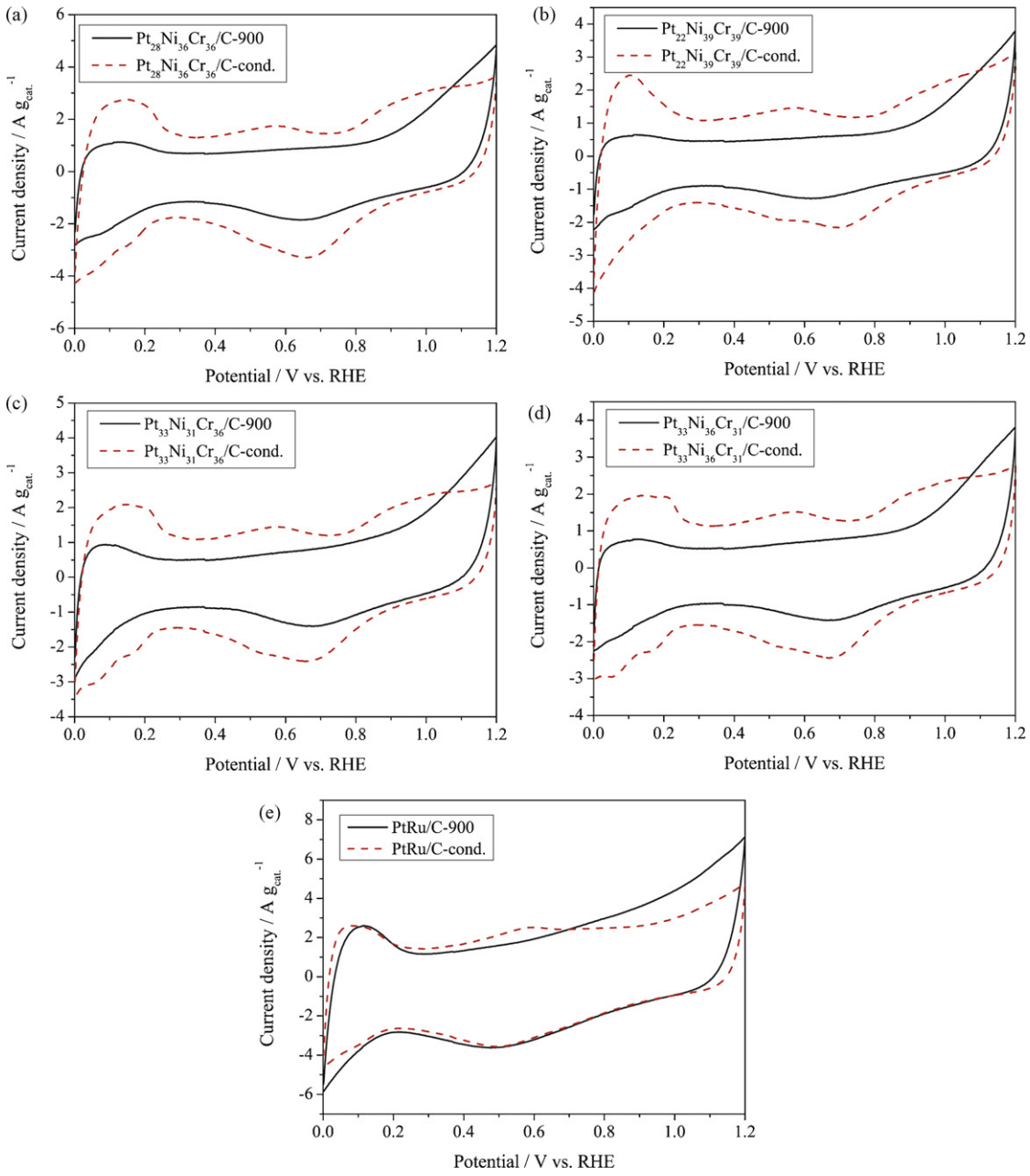

Fig. 10. The effect of conditioning examined by measuring cyclic voltammetry of the (a) $Pt_{28}Ni_{36}Cr_{36}$/C, (b) $Pt_{22}Ni_{39}Cr_{39}$/C, (c) $Pt_{33}Ni_{31}Cr_{36}$/C, (d) $Pt_{33}Ni_{36}Cr_{31}$/C, and (e) PtRu/C catalysts before and after the conditioning test. The experiments were performed by potential cycling between 0 and 1.2 V (vs. RHE) for 50 cycles at a scan rate of 50 mV s^{-1}. 0.5 M H_2SO_4 solution was used as the electrolyte.

in the $Pt_{28}Ni_{72}$/C-cond. (147%) and $Pt_{28}Cr_{72}$/C-cond. (1240%) catalysts, which shows that the extent of dissolution was regulated by co-alloying of Ni and Cr. In contrast, in the PtRu/C catalyst the EAS slightly decreased after the conditioning test, which means agglomeration of nano-particles and surface segregation of Ru (hydrous) oxides occurred. The dissolution observed during conditioning suggests that further investigation of the long-term stability of the PtNiCr catalysts is needed to determine their suitability for extended use in fuel cells.

The MOR activity measurement results before and after the conditioning tests are shown in Fig. 11. Before the conditioning process, the order of MOR activity at 60 min operation time was: PtRu/C-900 (3.56 A $g_{cat.}^{-1}$) ≫ $Pt_{28}Ni_{36}Cr_{36}$/C-900 (1.09 A $g_{cat.}^{-1}$) > $Pt_{33}Ni_{31}Cr_{36}$/C-900 (0.938 A $g_{cat.}^{-1}$) > $Pt_{33}Ni_{36}Cr_{31}$/C-900 (0.564 A $g_{cat.}^{-1}$) ≫ $Pt_{22}Ni_{39}Cr_{39}$/C-900 (0.162 A $g_{cat.}^{-1}$). After the conditioning, the order of the MOR activity was changed to: PtRu/C-cond. (5.07 A $g_{cat.}^{-1}$) > $Pt_{28}Ni_{36}Cr_{36}$/C-cond. (4.03 A $g_{cat.}^{-1}$) > $Pt_{22}Ni_{39}Cr_{39}$/C-cond. (3.24 A $g_{cat.}^{-1}$) > $Pt_{33}Ni_{36}Cr_{31}$/C-cond. (2.88 A $g_{cat.}^{-1}$) > $Pt_{33}Ni_{31}Cr_{36}$/C-cond. (2.57 A $g_{cat.}^{-1}$). Although the MOR activity of the $Pt_{28}Ni_{36}Cr_{36}$/C catalyst significantly improved after the conditioning process, the activity was still lower than that of the PtRu/C catalyst. But it is clearly seen that the $Pt_{28}Ni_{36}Cr_{36}$/C catalyst exhibited the highest MOR activity among the ternary Pt–Ni–Cr catalysts, which is in good agreement with our previous thin film combinatorial library study [27]. It should be noted that the ternary catalysts showed higher MOR mass activity after the conditioning test than the 0.733 and 2.12 A $g_{cat.}^{-1}$ values of the $Pt_{28}Ni_{72}$/C-cond. and $Pt_{28}Cr_{72}$/C-cond. catalysts, respectively. This demonstrates the synergistic effect of co-alloying of Ni and Cr into Pt. In addition, these results highlight a principal benefit of a

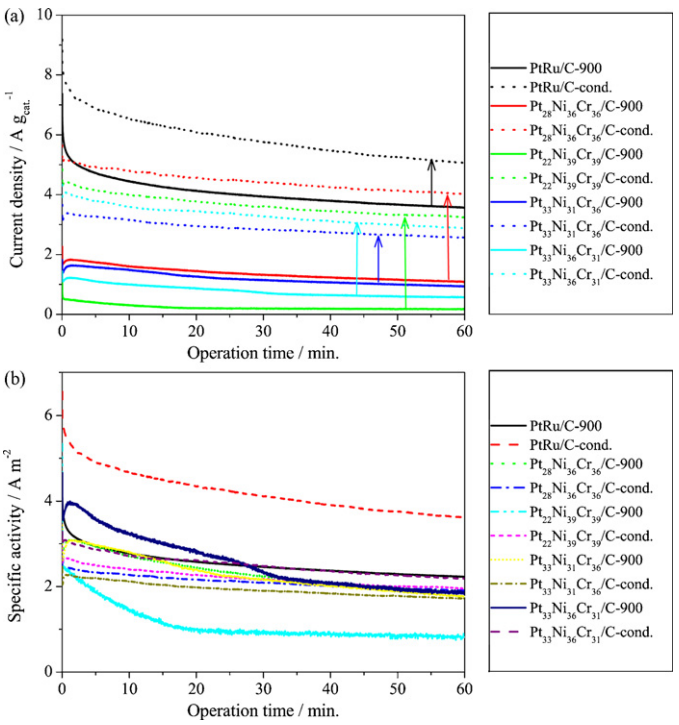

Fig. 11. Chronoamperometry test results of the ternary catalysts before and after the conditioning tests based on (a) catalyst mass activity (A $g_{cat.}^{-1}$) and (b) specific activity (A m^{-2}). 1 M methanol + 1 M H_2SO_4 solution was used as the electrolyte. The tests were performed by keeping the working electrodes at 0.6 V (vs. RHE) for 60 min.

combinatorial synthesis and high-throughput screening method: fast identification of promising compositions.

Specific activities are shown in Fig. 11(b). A dramatic increase of the MOR specific activity was observed in the PtRu/C-cond. (62%) and $Pt_{22}Ni_{39}Cr_{39}$/C-cond. (150%) catalysts, while only a slight increase was observed in the other catalysts. In the case of the PtRu/C catalyst, this increase in the specific MOR activity comes from a change of the Ru oxidation state [38–40]. The especially large increase of the specific activity in the $Pt_{22}Ni_{39}Cr_{39}$/C-cond. catalyst can be rationalized by the significantly low specific activity of the $Pt_{22}Ni_{39}Cr_{39}$/C-900 catalyst, although the reason for the poor performance in this catalyst is not clear. It should be noted that all of the conditioned Pt–Ni–Cr catalysts show close specific activities (1.72–2.18 A m^{-2}) and the increase of the specific activities after the conditioning process was not significant. Recalling that the specific activities of $Pt_{28}Ni_{72}$/C-cond. and $Pt_{28}Cr_{72}$/C-cond. were 1.46 and 2.20 A m^{-2}, respectively, we can conclude that the co-alloying did not cause a synergistic effect in specific activity. But it is interesting to compare the EAS values of the conditioned catalysts: it was 0.501 and 0.962 m^2 $g_{cat.}^{-1}$ in the $Pt_{28}Ni_{72}$/C-cond. and $Pt_{28}Cr_{72}$/C-cond., respectively, which increased to 2.11, 1.66, 1.49, and 1.32 m^2 $g_{cat.}^{-1}$ in the $Pt_{28}Ni_{36}Cr_{36}$/C-cond., $Pt_{22}Ni_{39}Cr_{39}$/C-cond., $Pt_{33}Ni_{31}Cr_{36}$/C-cond., and $Pt_{33}Ni_{36}Cr_{31}$/C-cond. catalysts, respectively. These results show that after conditioning, the ternary catalysts have larger EAS values than the binary catalysts although the ternary ones have lower Cr content than the $Pt_{28}Cr_{72}$/C-cond. catalyst. These results suggest that the high MOR activity in the ternary catalysts came from the co-alloying of Ni and Cr which produced more exposure of Pt on the catalyst surface without losing specific activities during the conditioning process. The improved activity of the binary and ternary catalysts studied in this paper could result from both the well-known bi-functional mechanism [41] and an electronic (ligand) effect [42]. Deeper analysis of the reaction mechanism is needed to clarify contribution of each mechanism as the two mechanisms are hard to distinguish [43].

It should be mentioned that the highest MOR mass activity among the conditioned binary and ternary Pt–Ni–Cr catalysts was observed in the $Pt_{28}Ni_{36}Cr_{36}$/C-cond. catalyst in spite of similar specific activities for all the samples. The order of mass activity of the as-prepared catalysts were $Pt_{28}Ni_{36}Cr_{36}$/C > $Pt_{33}Ni_{36}Cr_{31}$/C > $Pt_{22}Ni_{39}Cr_{39}$/C > $Pt_{33}Ni_{31}Cr_{36}$/C > $Pt_{28}Cr_{72}$/C > $Pt_{28}Ni_{72}$/C. After the conditioning, the order changed to: $Pt_{28}Ni_{36}Cr_{36}$/C-cond. > $Pt_{22}Ni_{39}Cr_{39}$/C-cond. > $Pt_{33}Ni_{36}Cr_{31}$/C-cond. > $Pt_{33}Ni_{31}Cr_{36}$/C-cond. > $Pt_{28}Cr_{72}$/C-cond. > $Pt_{28}Ni_{72}$/C-cond., with only the $Pt_{22}Ni_{39}Cr_{39}$ and $Pt_{33}Ni_{36}Cr_{31}$ compositions changing their positions. These results mean that (1) non-annealed catalysts and conditioned catalysts have similar ordering of MOR mass activity and (2) the $Pt_{28}Ni_{36}Cr_{36}$ composition is an optimum composition in both the non-annealed and conditioned forms, although reaction mechanism in each form might be different. In addition, these results suggest that anodic conditioning of a thin film combinatorial library can help to improve the performance correlation between thin films and as-prepared powder catalysts, and that use of a conditioning process should always be considered in evaluating sputter deposited combinatorial libraries.

As noted above, the PtNiCr powder catalyst activity rankings correlate well with thin film activity screening results. The superior performance of the Pt–Ru catalyst powders also mirrors the performance seen in thin film screening across many systems. The compositions that have shown the strongest peak current densities along with low MOR onset potentials have all been in Ru-containing ternary systems [44]. This is further evidence of the unique role of Ru in enhancing MOR performance in alloy systems.

Finally, from a practical viewpoint, it is also useful to compare the MOR activities on a g-noble metal scale (A $g_{nobl\,metal}^{-1}$) as the noble metal cost plays a major part in price determination. The MOR activity of the $Pt_{28}Ni_{36}Cr_{36}$/C catalyst was 38.2 A $g_{noble\,metal}^{-1}$, while that of the PtRu/C catalyst was only half of this value (17.9 A $g_{noble\,metal}^{-1}$). All the other ternary catalysts considered here also performed significantly better than the PtRu/C catalyst in this regard (see Table 2). The $Pt_{28}Ni_{72}$/C (17.3 A $g_{noble\,metal}^{-1}$) and $Pt_{28}Cr_{72}$/C (17.5 A $g_{noble\,metal}^{-1}$) catalysts did not show improved MOR activity in this respect. These results suggest that the ternary Pt–Ni–Cr catalysts are promising candidates for the MOR in DMFCs, especially where catalyst cost is a major issue.

4. Conclusion

Various compositions of ternary Pt–Ni–Cr and binary PtNi and PtCr catalysts were investigated to verify the composition dependence for the MOR suggested by earlier thin film studies. The $Pt_{28}Ni_{36}Cr_{36}$ composition showed the highest MOR mass activity (4.42 A $g_{cat.}^{-1}$) among the binary and ternary compositions in their as-prepared form during chronoamperometry testing (0.6 V and 60 min), which was even better than the PtRu/C catalyst (3.58 A $g_{cat.}^{-1}$). The $Pt_{28}Ni_{36}Cr_{36}$ composition showed its highest MOR activity among the alloys both before and after the conditioning process. The order of mass activity before ($Pt_{28}Ni_{36}Cr_{36}$/C > $Pt_{33}Ni_{36}Cr_{31}$/C > $Pt_{22}Ni_{39}Cr_{39}$/C > $Pt_{33}Ni_{31}Cr_{36}$/C > $Pt_{28}Cr_{72}$/C > $Pt_{28}Ni_{72}$/C) and after ($Pt_{28}Ni_{36}Cr_{36}$/C-cond. > $Pt_{22}Ni_{39}Cr_{39}$/C-cond. > $Pt_{33}Ni_{36}Cr_{31}$/C-cond. > $Pt_{33}Ni_{31}Cr_{36}$/C-cond. > $Pt_{28}Cr_{72}$/C-cond. > $Pt_{28}Ni_{72}$/C-cond.) the conditioning process was very similar. The increase in both the EAS values and specific activities of the binary $Pt_{28}Ni_{72}$/C-cond. and $Pt_{28}Cr_{72}$/C-cond. catalysts revealed that both Ni (metallic Ni) and Cr (Cr_2O_3) experienced dissolution and oxidation state change during the conditioning process, with the dissolution being more significant in Cr_2O_3, while the increase of specific activity was higher in metallic Ni. The close specific activity results of all the ternary catalysts showed that their improved mass activity came from the increase in the EAS and that co-alloying of Ni and Cr could provide a synergistic

effect by exposing more Pt on the catalyst surface than in the binary catalysts without losing their intrinsic activity during the conditioning process.

Acknowledgements

This work was partially supported by the U.S. Army CECOM RDEC through Agreement DAAB07-03-3-K414 and by the Department of Defense and the Army Research Office through contract numbers W911QX06C0117 and W911NF08C0037. Such support does not constitute endorsement by the U.S. Army of the views expressed in this publication.

References

[1] A.S. Arico, S. Srinivasan, V. Antonucci, Fuel Cells 1 (2001) 133–161.
[2] M. Watanabe, S. Motoo, J. Electroanal. Chem. 60 (1975) 267–273.
[3] N.M. Markovic, H.A. Gasteiger, P.N. Ross Jr., Electrochim. Acta 40 (1995) 91–98.
[4] W. Chrzanowski, A. Wieckowski, Langmuir 14 (1998) 1967–1970.
[5] O.A. Petrii, J. Solid State Electrochem. 12 (2008) 609–642.
[6] E. Antolini, Appl. Catal. B: Environ. 74 (2007) 324–336.
[7] C. Lamy, A. Lima, V. LeRhun, F. Delime, C. Coutanceau, J.-M. Léger, J. Power Sources 105 (2002) 283–296.
[8] U.B. Demirci, J. Power Sources 173 (2007) 11–18.
[9] M.K. Jeon, J.Y. Won, K.R. Lee, S.I. Woo, Electrochem. Commun. 9 (2007) 2163–2166.
[10] M.K. Jeon, K.R. Lee, H. Daimon, A. Nakahara, S.I. Woo, Catal. Today 132 (2008) 123–126.
[11] J.-H. Choi, K.-W. Park, B.-K. Kwon, Y.-E. Sung, J. Electrochem. Soc. 150 (2003) A973–A978.
[12] Z.B. Wang, G.P. Yin, P.F. Shi, Y.C. Sun, Electrochem. Solid State Lett. 9 (2006) A13–A15.
[13] S. Pasupathi, V. Tricoli, J. Solid State Electrochem. 12 (2008) 1093–1100.
[14] J.S. Cooper, P.J. McGinn, J. Power Sources 163 (2006) 330–338.
[15] P. Strasser, Q. Fan, M. Devenney, W.H. Weinberg, P. Liu, J.K. Nørskov, J. Phys. Chem. B 107 (2003) 11013–11021.
[16] Z. Jusys, T.J. Schmidt, L. Dubau, K. Lasch, L. Jörissen, J. Garche, R.J. Behm, J. Power Sources 105 (2002) 297–304.
[17] M. Umeda, H. Ojima, M. Mohamedi, I. Uchida, J. Power Sources 136 (2004) 10–15.
[18] A. Oliveira Neto, E.G. Franco, E. Arico, M. Linardi, E.R. Gonzalez, J. Eur. Ceram. Soc. 23 (2003) 2987–2992.
[19] M.K. Jeon, K.R. Lee, K.S. Oh, D.S. Hong, J.Y. Won, S. Li, S.I. Woo, J. Power Sources 158 (2006) 1344–1347.
[20] M.K. Jeon, J.Y. Won, K.S. Oh, K.R. Lee, S.I. Woo, Electrochim. Acta 53 (2007) 447–452.
[21] P. Piela, C. Eickes, E. Brosha, F. Garzon, P. Zelenay, J. Electrochem. Soc. 151 (2004) A2053–A2059.
[22] Y. Chung, C. Pak, G.S. Park, W.S. Jeon, J.R. Kim, Y. Lee, H. Chang, D. Seung, J. Phys. Chem. C 112 (2008) 313–318.
[23] E. Antolini, J.R.C. Salgado, E.R. Gonzalez, Appl. Catal. B: Environ. 63 (2006) 137–149.
[24] C. Roychowdhury, F. Matsumoto, V.B. Zeldovich, S.C. Warren, P.F. Mutolo, M. Ballesteros, U. Wiesner, H.D. Abruna, F.J. DiSalvo, Chem. Mater. 18 (2006) 3365–3372.
[25] S. Papadimitriou, A. Tegou, E. Pavildou, G. Kokkinidis, S. Sotiropoulos, Electrochim. Acta 52 (2007) 6254–6260.
[26] Z. Liu, B. Guo, S.W. Tay, L. Hong, X. Zhang, J. Power Sources 184 (2008) 16–22.
[27] J.S. Cooper, M.K. Jeon, P.J. McGinn, Electrochem. Commun. 10 (2008) 1545–1547.
[28] M.K. Jeon, Y. Zhang, P.J. McGinn, Electrochim. Acta 54 (2009) 2837–2842.
[29] M.K. Jeon, P.J. McGinn, J. Power Sources 188 (2009) 427–432.
[30] M.K. Jeon, J.S. Cooper, P.J. McGinn, J. Power Sources 192 (2009) 391–395.
[31] B.C. Chan, R. Liu, K. Jambunathan, H. Zhang, G. Chen, T.E. Mallouk, E.S. Smotkin, J. Electrochem. Soc. 152 (2005) A594–A600.
[32] E.S. Smotkin, R.R. Diaz-Morales, Annu. Rev. Mater. Res. 33 (2003) 557–579.
[33] M.-S. Hyun, S.-K. Kim, B. Lee, D. Peck, Y. Shul, D. Jung, Catal. Today 132 (2008) 138–145.
[34] T.J. Schmidt, H.A. Gasteiger, G.D. Stäb, P.M. Urban, D.M. Kolb, R.J. Behm, J. Electrochem. Soc. 145 (1998) 2354–2358.
[35] C.Z. He, H.R. Kunz, J.M. Fenton, J. Electrochem. Soc. 144 (1997) 970–979.
[36] M.K. Jeon, J.S. Cooper, P.J. McGinn, J. Power Sources 185 (2008) 913–916.
[37] T. Biegler, D.A.J. Rand, R. Woods, J. Electroanal. Chem. 29 (1971) 269–277.
[38] D.R. Rolison, P.L. Hagans, K.E. Swider, J.W. Long, Langmuir 15 (1999) 774–779.
[39] J.W. Long, R.M. Stroud, K.E. Swider-Lyons, D.R. Rolison, J. Phys. Chem. B 104 (2000) 9772–9776.
[40] M.K. Jeon, J.Y. Won, S.I. Woo, Electrochem. Solid State Lett. 10 (2007) B23–B25.
[41] H.A. Gasteiger, N. Markovic, P.N. Ross, E.J. Cairns, J. Phys. Chem. 97 (1993) 12020–12029.
[42] J.A. Rodriguez, D.W. Goodman, Science 257 (1992) 897–903.
[43] M.A. Rigsby, W.-P. Zhou, A. Lewera, H.T. Duong, P.S. Bagus, W. Jaegermann, R. Hunger, A. Wieckowski, J. Phys. Chem. C 112 (2008) 15595–15601.
[44] J.S. Cooper, Combinatorial screening of fuel cell catalysts, Ph.D. Thesis, University of Notre Dame, Indiana, 2007.